SCIENTIFIC REPORTS

OPEN

Single electron-photon pair creation from a single polarization-entangled photon pair

Kazuyuki Kuroyama[1], Marcus Larsson[1], Sadashige Matsuo[1], Takafumi Fujita[1], Sascha R. Valentin [2], Arne Ludwig [2], Andreas D. Wieck[2], Akira Oiwa[3] & Seigo Tarucha[1,4]

Quantum entanglement between different forms of qubits is an indication of the universality of quantum mechanics. Entanglement transfer between light and matter, especially photon and spin, has long been studied as the central concept, but it remains technically challenging for single photons and spins. In this paper, we show paired generation of a single electron in a GaAs quantum dot and a single photon from a single polarization-entangled photon pair. We measure temporal coincidence between the single photo-electron detection and the single photon detection. Considering a single photon polarization is converted to an electron spin via an optical selection rule, the present result indicates the capability of photon to spin entanglement transfer. This may be useful to explore the physics of entanglement transfer and also for applications to quantum teleportation based quantum communication.

Entanglement transfer between light and matter has long been studied in order to explore fundamentals of quantum physics[1]. Moreover, this phenomenon is expected to be an important ingredient to realize distributed photonic quantum communication based on quantum repeaters but not yet well exemplified[2,3]. Coherent transfer of single-particle states between different kinds was previously demonstrated for a single photon to a single ion trapped in a Paul trap and Doppler cooled[4]. In addition, entanglement generation between a single photon and a single atom was performed using photon emission from the atom[5,6]. An electron spin or a hole spin confined in a semiconductor quantum dot has been regarded as one of the best candidates to engineer entanglement between a solid-state quantum and a photonic quantum. Indeed, experiments on entanglement generation has been reported for a photon emitted from an InGaAs self-assembled quantum dot (QD) and a remaining electron spin in it[7,8] and also for an InAs QD and a remaining electron spin[9]. However, direct experimental demonstration of entanglement transfer from photons to solid-state spins or vice versa remains challenging. Achieving this provides more variations of entanglement engineering between distant spins as well as between a photon and a spin spatially separated. Especially projection of single entangled photon pairs to single distant electron spin pairs in nano-scale quantum devices may provide a new tool to study non-local entanglement in mesoscopic solid-state physics.

Quantum state transfer of light to spin in solid[10] was experimentally demonstrated for ensembles of photon polarization states and electron spin states with a GaAs quantum well[11,12]. For the single-particle states we previously demonstrated angular momentum transfer from polarization of a single photon to spin of a single electron using GaAs QDs[13]. This implies that single polarization-entangled photon pairs can be used as a source to establish photon-spin entanglement and spin-spin entanglement for single photo-electrons trapped by QDs. However, no experiments on such photo-electron generation in QDs have been reported to date. Note the GaAs QDs[14] may have advantages compared to the self-assembled QDs in the ability of quantum gating[15,16] and scale-up[17–20], both of which are needed to combine the quantum communication with gate-based computation, but still challenging in self-assembled QDs.

In this paper, we report on the experimental observation of coincident generation of a photo-electron in a GaAs dot and a photon in a photo-detector from a polarization-entangled photon pair. One of the paired

[1]Department of Applied Physics, The University of Tokyo, Bunkyo-ku, Tokyo, Japan. [2]Lehrstuhl für Angewandte Festkörperphysik, Ruhr-Universität, Bochum, Germany. [3]The Institute of Scientific and Industrial Research, Osaka University, Ibaraki, Osaka, Japan. [4]Center for Emergent Materials Science, RIKEN, Wako, Saitama, Japan. Correspondence and requests for materials should be addressed to K.K. (email: kuroyama@meso.t.u-tokyo.ac.jp) or S.T. (email: tarucha@ap.t.u-tokyo.ac.jp)

Section I: Optical setup for SPDC   Section II: QD irradiation
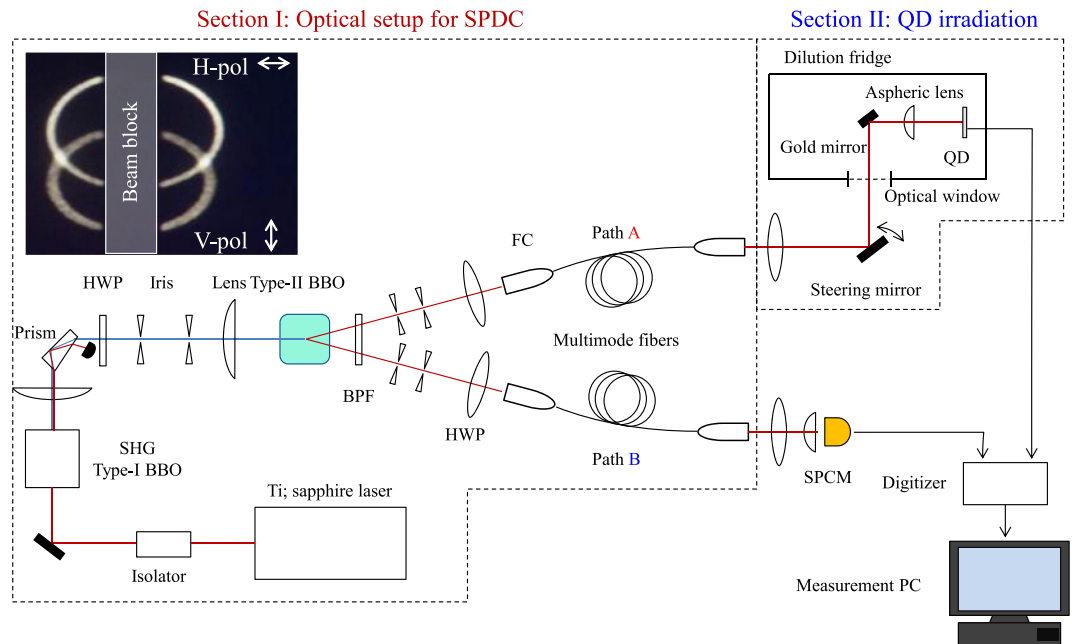
Figure 1. Experimental setup for a single photo-electron-photon pair creation and detection. Schematic of the experiment setup used for the coincidence measurement of the photo-electron excited in the dot and the photon at SPCM. The setup can be separated into two sections, I and II. Section I is an optical setup to generate paired photons by SPDC. A Ti:sapphire ultra-short pulsed laser is used to generate SHG photons with a Type-I BBO crystal. The SHG photons are irradiated on a Type-II BBO crystal to generate SPDC photons after removing the original laser light with a prism and two irises, and rotating the polarization with a half wave plate (HWP) to satisfy the phase matching condition of SPDC. The paired photons are emitted in two different SPDC photon cones through a band pass filter (BPF). A series of irises are placed to cut out the crossing points of the photon cones. After filtering the energy and the spatial position, the photons are coupled to the multimode fibers. The fiber output photons are observed by SPCM. Section II is a setup for irradiating the photons on the dot and detecting the photo-electron. The dilution refrigerator has an optical window at the bottom and the irradiating photons along Path A are focused by an aspheric lens on the sample through this optical window. The position of the irradiating photon spot can be aligned by tilting a steering mirror. Finally, the charge sensing signal of detecting the photo-electrons and the SPCM signal of counting the photons are monitored by the digitizer. The inset is a far-field image of the SPDC photons observed by a near infrared sensitive CCD camera. The upper, and the lower ring indicate the emission of horizontally polarizing photons, and vertically polarizing photons, respectively.

photons is irradiated on the GaAs QD, while the other on a single photon counter. Real-time measurements of the photo-electron in the dot by a charge sensor[21–26] and the photon by the photon counter are performed simultaneously to identify the temporal coincidence between the photo-electron detection and the photon detection. Although a fast real-time detection technique of an electron has been established for gate defined QDs in recent years, photo-electron detection is still technically difficult because QDs made in a doped quantum well becomes eventually unstable due to charge noise and persistent photo-conductivity when shining light pulses. To minimize such instability we irradiate photons with sufficiently weak intensity. The averaged interval of single photons irradiated on the dot and the photon counter is adjusted to be larger than the time resolution of the charge sensor and much larger than that of the photon counter. Therefore zero to two photons (N = 0 to 2) are mostly detected by the photon counter in a time window for detecting the photo-electron by the charge sensor. However, this does not always guarantee the detected photo-electrons and photons are originated from the same entangled photon pairs. By comparing the probability of detecting zero to two photons between with and without the photo-electron detection we are able to confirm coincident detection of a photo-electron and a photon from the same polarization-entangled photon pair. Because we already know in our previous experiment that a photon polarization is transferred to a spin angular momentum of a photo-electron[13], the present result provides a critical technical step for creation of an electron spin entanglement induced by a polarization-entangled photon pair and for applications to distributed quantum communication.

Setup
Optical setup for Spontaneous Parametric Down Conversion.
Figure 1 schematically shows the experimental setup consisting of two sections: Section I for generating single photon pairs using a spontaneous parametric down conversion (SPDC) technique[27,28] and Section II for detecting photo-electrons in the dot and photons by the photon counter upon separate irradiation of single photons from the photon pairs.

A Ti:sapphire ultra-short pulsed laser (MIRA-900P) with auto-correlation width of 3 psec and repetition rate of 76 MHz is used to generate the SPDC photons. The laser pulse has a peak power of 2 kW with the center

wavelength of 808 nm (1.5345 eV). This wavelength is adjusted to coincide with the excitation energy for the heavy hole (HH) exciton in the GaAs QD. The photon energy is doubled via second harmonic generation (SHG) using a Type-I Beta-Barium-Borate (BBO) crystal. To extract only the SHG photons a Pellin-Broca prism, several irises and short pass filters are used. The average power of the filtered second harmonic light obtained is about 100 mW. The SHG photons are irradiated on a Type-II BBO crystal in order to generate SPDC photon pairs. A band pass filter whose transmittance is maximal at 800 nm is placed just after the crystal to only transmit the SPDC photon pairs. The paired photons have two kinds of linear polarization orthogonal to each other and are emitted in two different directions. The inset of Fig. 1 shows the far-field image of the emitted photons observed by a CCD camera. The upper and lower ring indicate the horizontally, and vertically polarized photons, respectively. The polarization of the photons coming on the crossing points of the two rings cannot be distinguished, and therefore the paired photon state is polarization-entangled as represented by $(|HV\rangle + |VH\rangle)/\sqrt{2}$, where $|H\rangle$ and $|V\rangle$ indicate the horizontally and vertically linearly polarized photon state, respectively. A series of two irises are placed on each crossing point behind the band pass filter to extract the paired photons that are entangled but emitted in two directions, and the photons are separately coupled into two multimode fibers whose core diameter is 50 μm. Here we call the photon path through the right (left) crossing point of the two photon rings as Path A (B).

In order to confirm the polarization correlation of the paired photons we executed a coincidence measurement between the optical fiber outputs. Each output is detected by an avalanche photodiode mounted on a single photon counting module (SPCM). The SPCM signal, synchronized with repeating pulses of the Ti:sapphire laser, is counted using a PCI board (Time Harp 200, Pico Quanta). To selectively pick up the coincidence signals, a logical AND is performed on the two different SPCM signals or two optical fiber outputs. From the polarization correlation measurement taken on the coincidence photons (see SI), we confirmed that the detection rate of the entangled photon pairs is 14 to 16 kHz.

GaAs lateral quantum dot.

The GaAs QD device used for trapping single photons is defined by surface Schottky gates in a two-dimensional electron gas formed in a 15 nm thick GaAs well located between two thick $Al_{0.33}Ga_{0.67}As$ barriers (see Fig. 2(a,b))[29,30]. To enhance the efficiency of photon absorption in the dot, a distributed Bragg reflector (DBR) consisted of multiple $Al_{0.10}Ga_{0.90}As/AlAs$ bi-layers is embedded. For the photon trapping experiment a single QD is formed by applying appropriate negative voltages to the gates to deplete the carrier density underneath them and in their direct surrounding. On both side of the QD, additional dots are placed as charge sensors[31,32], but only the right charge sensor is used in the experiment here. In addition a 300 nm thick Au/Ti mask (not seen in Fig. 2(b)) having a 500 nm-diameter aperture is placed on top of the photon-electron trapping QD to avoid photon irradiation on the device area outside the dot. All measurements are carried out for the dot device placed in a dilution refrigerator (TRITON 200) at a base temperature of 25 mK. The photons are irradiated on the dot through an optical window equipped at the bottom of the fridge. The single photo-generated electron is detected by measuring the QD charge sensor response upon the photon irradiation. A change in the number of electrons in the dot modifies the charge sensor current, I_{sensor}, which is measured using a radio frequency reflectometry technique, which we call: rf-QD[33]. We set the QD sample into a RF-circuit which shows resonance at 215.5 MHz. The minimal charge detection time achieved is 10 μsec limited by the time of integration of I_{sensor} needed to keep the signal-to-noise ratio $10 \times \log_{10}(I_{sensor\_signal}/I_{sensor\_noise})$ higher than 0 dB. Note that the RF-circuit response time is much less than 10 μsec.

The QD charge state as a function of gate voltages can be determined using the charge sensor as shown in Fig. 2(c). Differential conductance dI_{sensor}/dV_R of the charge sensor versus two gate voltages V_R and V_L is shown without the photon irradiation. Sharp lines indicated by arrows are the charge state transition lines separated by the sum of the Coulomb gap and the QD level spacing. The lowest line indicates the transition between the zero and one electron state in the dot, and the number of electrons in the dot increases one-by-one every time when crossing the transition line upward. Figure 2(d) shows the real time trace of I_{sensor} measured on one of the transition lines. Transitions between the two current values indicate the charge tunnelling between the dot and the source or drain electrode. The time scale of electron trapping can be evaluated from the time interval needed for I_{sensor} switching from the lower level of about 0.05 to the higher level of about 0.09. Note that value of I_{sensor} depends on the gate bias position of the charge sensor because the charge sensor conductance shows Coulomb oscillations as seen in the background in Fig. 2(c).

In the photon irradiation experiment we adjusted the electron trapping time to a few hundred micro seconds which is about ten times longer than the averaged interval of the down converted photons. The charge state is tuned to be in the Coulomb gap or roughly 0.5 meV below the Fermi energy of the contact leads (green circle in Fig. 2(c))[34]. This energy is much larger than the electron temperature of 100 mK in the contact leads.

The mechanism of photo-electron trapping in this experiment is explained in detail in ref.[26]. Photo-electrons are created in the dot by optical excitation of electron-hole pairs in the GaAs QW at the Γ-point. The dot is confined laterally by a electro-static potential and vertically by the AlGaAs/GaAs/AlGaAs double heterostructure, so that the photo-generated electron remains in the dot being trapped by the lateral potential whereas the hole laterally escapes from the dot.

Results

Coincidence measurement on the electron and the photon.

Next, we generate photon pairs and irradiate one of the paired photons on the dot in Path A and the other on SPCM in Path B. A photo-electron is generated in the dot and detected by the charge sensor as shown in Fig. 2(d), leaving the photon detection setup of Path B unchanged. The charge sensor signal, I_{sensor} and the photon counter signal, V_{photon} are both monitored using a digitizer whose data acquisition rate is 100 MHz. The integration time of I_{sensor}, and V_{photon} is 10 μsec, and 10 nsec, respectively.
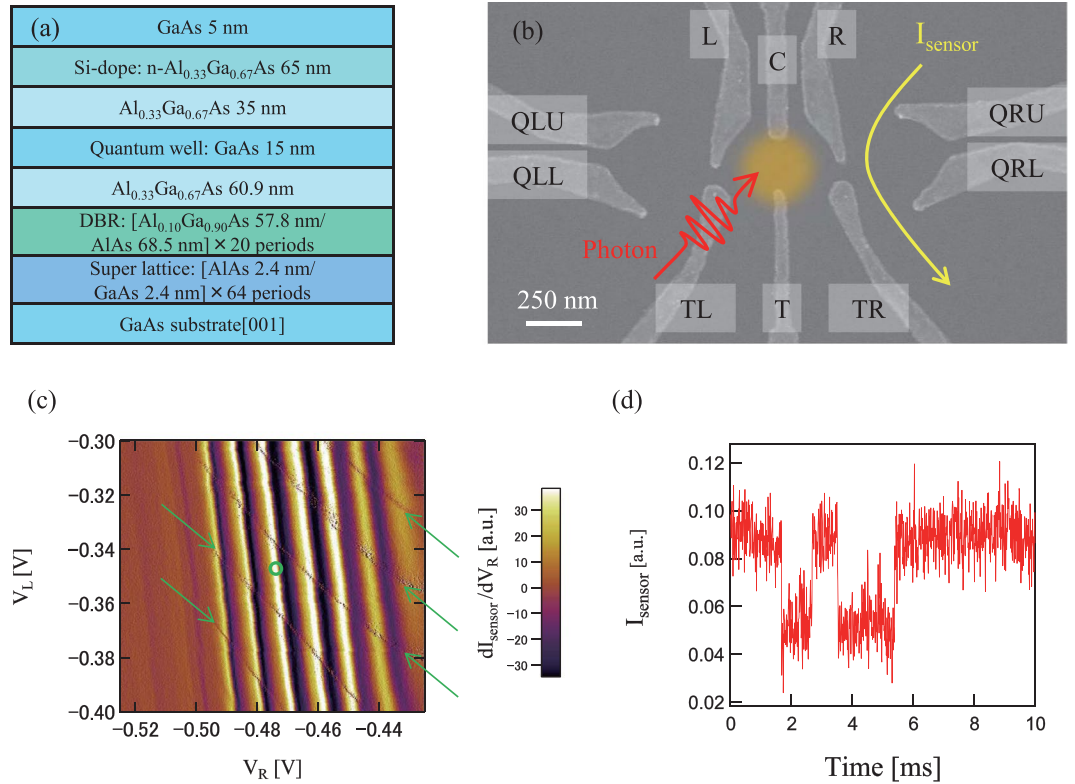
Figure 2. QD formation in the GaAs/AlGaAs heterostructure QW. (**a**) Layer profile of the quantum well wafer used for fabricating the QD device. A 15 nm GaAs well is sandwiched by two thick barrier layers of $Al_{0.33}Ga_{0.67}As$. Below the barrier layer a DBR structure consisting of periodic $Al_{0.10}Ga_{0.90}As$/AlAs quarter-wave stacks is embedded. (**b**) Scanning electron micrograph of a test device fabricated in the same way. The dot position formed by surface gates is pictorially shown by the orange circle. On the right side of the dot, an additional dot is formed as a charge sensor and its conduction is measured by a RF circuit. (**c**) Typical stability diagram of the single dot characterized by the differential conductance of the charge sensor current, dI_{sensor}/dV_R as a function of two gate voltages V_L and V_R. The thin gray lines indicated by the green arrows are the charge transition lines of the photo-electron trapping QD. We set the gate voltages V_L and V_R at the green circle position between the charge transition lines for the photon irradiation experiment. (**d**) Typical time trace of the single electron tunnelling between the dot and source-drain electrodes. When the electron enters (leaves) the dot, I_{sensor} abruptly drops (rises). The time trace is taken over 10 μsec for integrating the I_{sensor} data.

In order to obtain the photo-electron trapping efficiency η_{QD} we separately performed a single pulse excitation experiment. We first evaluated the light transmission through the metal mask aperture above the dot (described before). On the other hand, the laser beam spot size on the metal mask is approximately 10 μm. Thus we could derive the transmission coefficient T_{aper} of about 0.25% although it is difficult to discuss sub-wavelength hole transmission coefficient[35].

In addition, we tune pulsed laser intensity by using several neutral density filters such that a few to a few tens of photons go through the optical mask on top of the dot in each pulse irradiation. A single light pulse is picked up from the pulse train with an acoustic optical modulator(AOM) which is triggered by an external logical signal. We count the photo-electron trapping events which are detected synchronously detected by the charge sensor with the laser pulsing on the QD. Finally η_{QD} is obtained by calculation using the following equation.

$$\eta_{QD} = \frac{\text{(the number of photo} - \text{electron trapping events)}}{\text{(the number of pulse irradiations)} \times \text{(photon number in a single pulse)} \times T_{aper}} \tag{1}$$

The efficiency of photo-electron trapping by the dot depends on the incident photon energy on the dot as shown in Fig. 3(a). The efficiency is evaluated for the incident photons which pass through the optical mask above the dot and is contained in a single light pulse (see SI). The efficiency is maximum of 0.15% for the resonant excitation of heavy hole excitons at 1.534 eV. We additionally measure photo-luminescence spectrum(PL) on the same QW wafer at 77 K. The resonance energy of the HH exciton as shown in Fig. 3(a) is consistent with the PL spectrum (see SI). Besides, we previously experimentally verified HH and LH resonant excitation on GaAs lateral QDs[26], and the resonance peak in Fig. 3(a) is similar to the reported result. In the following experiment, we set the laser photon energy (1.5345 eV) resonating with the HH excitons.

Figure 3(b,c) show the time traces of I_{sensor} and V_{photon} measured simultaneously: red circles for I_{sensor} and green spikes for V_{photon}. Each V_{photon} spike indicates a single photon detection by the single photon counter. The I_{sensor}

(a)

(b) One coincidence photon

(c) Two coincidence photons
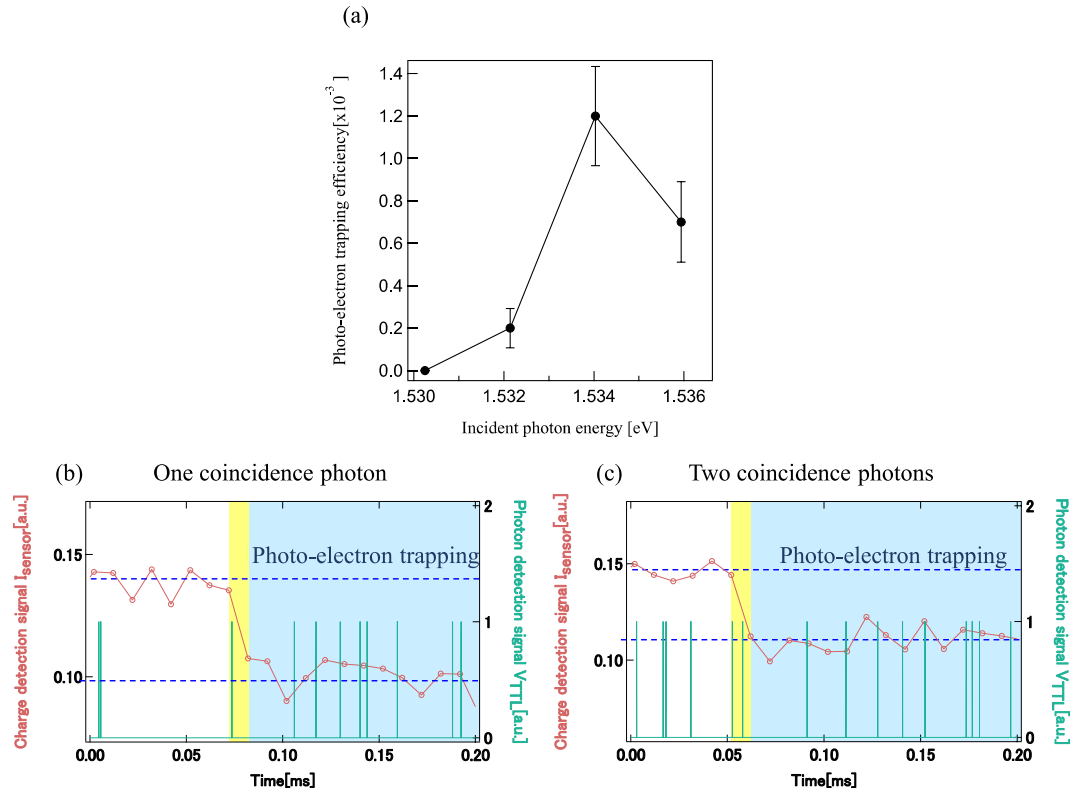
Figure 3. Quantum efficiency of the QD device and real-time measurement of a single photo-electron-photon pair. (**a**) Energy spectrum of photo-electron trapping efficiency on the QD taken under external in-plane magnetic field of 9 T. The horizontal axis is energy of incident photon. The peak at 1.534 eV corresponds to resonant excitation of the heavy hole exciton. (**b,c**) Examples of simultaneously measured time traces for the charge sensor current I_{sensor} in red and the SPCM photon detection signal V_{photon} in green. One photon and two photons are detected by the SPCM in the 10 μsec photon-electron trapping time window in yellow of photon trapping by the dot in (**b,c**), respectively. The I_{sensor} falls indicate that one photo-electron is trapped by the dot at some point in the time window.

time trace measured upon the photo-electron trapping is similar to that of Fig. 2(d). I_{sensor} abruptly decreases to the low level upon photon irradiation and then stays at the low level, indicating that a single photo-electron is trapped by the dot in the 10 μsec time window of the yellow color and stays in the dot. In most cases one, or two V_{photon} spikes are detected at the SPCM in this time window as shown in (b), or (c), respectively. We repeated the experiments of separately irradiating paired photons on the dot and on the photon counter, and finally acquired 27 traces indicating the photo-electron trapping by the dot. We calculated the probability $P_{coinci}(N)$ of finding N (=0, 1, 2, …) photons in the 10 μsec trapping time window conditioned on single photo-electron detection at the dot. The obtained probabilities are $P_{coinci}(0) = 44\%$, $P_{coinci}(1) = 41\%$, and $P_{coinci}(2) = 15\%$. We estimate possible errors of $P_{coinci}(N)$ by assuming that the errors of the probabilities follow Gaussian distribution. The evaluated errors of $P_{coinci}(N)$ are 6.8 to 9.7% and 0.947 to 1.62%, respectively (See SI, Table SI1).

To examine the effect of dark counts in the charge sensing o the observed photo-electron trapping events we irradiated the SPDC photons on the outside of the optical mask aperture. Then we observed no trapping events for 1 hour time trace acquisition. Note that we observe on or two trapping events on average for the 10 sec time trace acquisition when the irradiating position is on the aperture. Therefore, we confirmed that the dark count effect can be neglected in the present setup for the QD charge state being deep in the Coulomb gap (see Fig. 2(c)).

Concerning the photon detector, the dark count rate is typically 50 Hz or at most 100 Hz, which is much less than the SPDC photon detection rate of a few ten to one hundred kHz. Therefore, we assume that the dark count effect can be neglected also for the photon detection.

To confirm if the obtained photo-electron trapping events are induced by SPDC photons or dark count, we irradiate the SPDC photons to outside the aperture on the optical mask. In a case that the irradiating position is on the aperture, 1 or 2 trapping events are observed during 10 sec irradiation. Otherwise, we do not see any trapping events for 1 hour time trace acquisition. The result indicates that when the QD is tuned in Coulomb blockade regime substantial influence from the dark counting in the charge sensor like accidental or spontaneous charging is completely suppressed while acquiring the simultaneous time traces.

Besides, dark counting rate of the photon detector is typically 50 Hz and at most 100 Hz. Because the rate is much less than SPDC photon detection rate of a few ten to one hundred kHz, we think that contribution of the dark counting on the photon detector to the result can also be ignored.
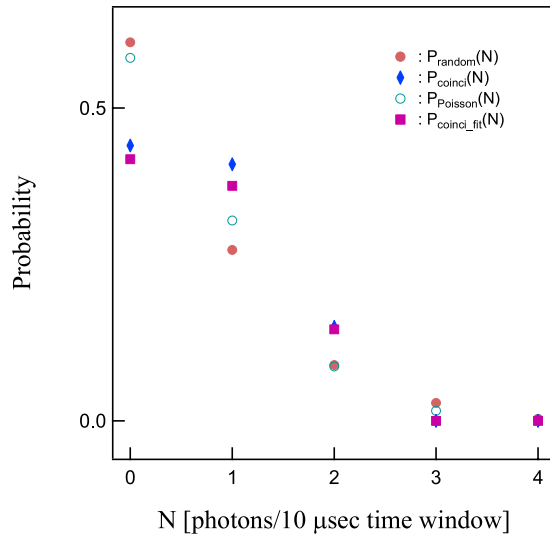
Figure 4. Comparison between $P_{coinci}(N)$ and $P_{random}(N)$, and best fits $P_{coinci\_fit}(N)$ to $P_{coinci}(N)$ with P_{el-ph} as a parameter. The N photon detection probability $P_{Posioon}(N)$ (green circles) calculated for a Poisson distribution with a 55 kHz average photon detection rate well reproduces $P_{random}(N)$ (orange circles). The least squared fits $P_{coinci\_fit}(N)$ (purple squares) to $P_{coinci}(N)$ (blue diamonds) is obtained using P_{el-ph} as a parameter. The statistics of $P_{coinci}(N)$ and $P_{coinci\_fit}(N)$ are significantly deviated from those of $P_{random}(N)$ and $P_{Poisson}(N)$, originating from creation of single pairs of a photo-electron and a photon.

Discussion

Probability of a single electron-photon pair creation. In Fig. 3(b) two photons are detected in the photo-electron trapping window. This occurs unintentionally because the time window is not small enough compared to the average interval of the photon counting signals. Note that the SPCM photon detection observed in the photo-electron trapping time window does not always indicate that the photo-electron in the dot detected by the charge sensor and the photon detected by SPCM are coincident or originated from the same SPDC photon pair because the generation efficiency of the entangled photon pairs is relatively low. To evaluate the probability of the non-coincident detection in $P_{coinci}(1)$ and $P_{coinci}(2)$ we derived the averaged probability $P_{random}(N)$ of detecting N = 0 to 2 photons per 10 μsec by the photon counter regardless of whether the photo-electron is detected or not. The obtained $P_{random}(0) = 60.5\%$, $P_{random}(1) = 27\%$ and $P_{random}(2) = 8.9\%$, respectively. Note that the photon counting rate for Path B measured just before the coincidence experiment is about 55 kHz. We calculate the probability $P_{Poisson}(N)$ of the photon detection in the 10 μsec time window using the Poisson statistics and find good agreement with $P_{random}(N)$ for N = 0 to 4 (See Fig. 4). Compared with these values of $P_{random}(1)$ and $P_{random}(2)$, $P_{coinci}(1)$ and $P_{coinci}(2)$ are significantly larger, but $P_{coinci}(0)$ is significantly smaller than $P_{random}(0)$, because of the contribution from the true coincident detection of a photon and a photo-electron generated from the same SPDC photon pair.

We estimate a conditional probability P_{el-ph} that a truly correlated photon is detected given that a photo-electron is detected by the QD charge sensor, by comparing $P_{coinci}(N)$ and $P_{random}(N)$. $P_{coinci}(N)$ and $P_{random}(0)$ directly related to each other with P_{el-ph} as a parameter:

$$P_{coinci}(0) = (1 - P_{el-ph}) \times P_{random}(0) \tag{2}$$

$$P_{coinci}(N) = P_{el-ph} \times P_{random}(N - 1) + (1 - P_{el-ph}) \times P_{random}(N) \text{ (For the case of } 1 \leqq N \leqq 4) \tag{3}$$

We use least squares method to fit these functions to the measured $P_{coinci}(N)$ to evaluate P_{el-ph}. The adapted values $P_{coinci\_fit}(N)$ for $P_{coinci}(N)$ with N = 0 to 4 by optimizing P_{el-ph} are shown by te purple symbols in Fig. 4. The best agreement between $P_{coinci\_fit}(N)$ and $P_{coinci}(N)$ is obtained with P_{el-ph} of 31%. This value is comparable to a probability of a paired photon detection evaluated at coincidence measurement of paired photons (See SI).

Further consideration about the result. By taking into account P_{el-ph}, we can evaluate the conversion efficiency from SHG to SPDC. The SHG average power P_{SHG} is roughly 100 mW and with the wavelength λ_{SHG} of 404 nm or the photon energy E_{SHG} of 3.0681 eV in energy. We use these values to calculate the SHG photon number Γ_{SHG} in 1 second using the following equation:

$$\Gamma_{SHG} = \frac{P_{SHG}}{E_{SHG} \times 1.602 \times 10^{-19}} \tag{4}$$

$$\simeq 2.0 \times 10^{17} \text{ [photons/sec]}, \tag{5}$$

where the factor of 1.602×10^{-19} is the scaling ratio between electron bolt and Joule.

The conversion efficiency ξ_{conv} from photon pair to electron-photon pair obtained here is mainly limited by the QD photon absorption coefficient η_{QD} of 1.2×10^{-3} (discussed before) and estimated by multiplying η_{QD} by the SPCM detection efficiency η_{SPCM} which is about 50% at 800 nm photon wavelength. Therefore we obtain $\xi_{conv} \simeq 6.0 \times 10^{-4}$.

Finally, we consider ways to improve the coincidence probability. Recent technical advances in rf-QDs charge sensing enable us to shorten the charge detection time down to 100 nsec[36]. If the charge detection time decreased to 1 μsec, one photon detection probability in a 1 μsec time window $P_{random}(1)$ can be suppressed down to 1/10 of the current value, while the probability of the true coincident events is unchanged. For the case of 55 kHz average photon detection rate and the 1 μsec time window, $P_{random}(0) = 95\%$, $P_{random}(1) = 5.2\%$ and $P_{random}(N \geqq 2)$ is less than 1%. This shortening of the time window indicates that probability of detecting only a truly correlated photon given that a photo-electron is detected can be enhanced. To increase the generation rate of the polarization-entangled photon pairs will also be efficient to raise the probability of finding the true coincident pairs of the photo-electron and the photon.

Summary

In summary, we performed the coincidence measurement of single photo-electrons in a quantum dot and single photons using a down converted polarization-entangled photon pair. We compared the probability of detecting the photon by the photon counter between with and without the photo-electron detection in the dot, and found the former to be substantially higher than the latter. From this comparison we estimated the coincidence rate to be comparable to the emission rate of the original photon pairs. We previously demonstrated that single electron spins are photo-generated in QDs by irradiating single photons with preserving the angular momentum. Consequently combining with the present result, we here presume that the angular momentum correlation is preserved between the single photo-electrons in the dot and the single photons that are spatially separated but generated from the same polarization-entangled photon pairs.

Methods

Device fabrication. Our device is fabricated from a GaAs/AlGaAs heterostructure wafer which defines a 2 DEG. The electron density and mobility in the 2 DEG are 1.91×10^{11} cm^{-2} and 1.24×10^{6} cm^2/V$\cdot$sec at 4.2 K, respectively. Surface Schottky fine gates of Au/Ti to define the QD are fabricated using electron beam lithography as shown in Fig. 2(b). The fine gates are covered with a 120 nm thick insulator layer of calixarene and a 300 nm thick Au/Ti mask, having a 500 nm-diameter aperture which is placed on top of the photon-trapping QD.

References

1. Hald, J., Sørensen, J., Schori, C. & Polzik, E. Entanglement transfer from light to atoms. *Journal of Modern Optics* **47**, 2599–2614, https://doi.org/10.1080/09500340008232184 (2000).
2. Gobby, C., Yuan, Z. L. & Shields, A. J. Quantum key distribution over 122 km of standard telecom fiber. *Applied Physics Letters* **84**, 3762–3764 (2004).
3. Briegel, H.-J., Dür, W., Cirac, J. I. & Zoller, P. Quantum Repeaters: The Role of Imperfect Local Operations in Quantum Communication. *Physical Review Letters* **81**, 5932–5935, https://doi.org/10.1103/PhysRevLett.81.5932, (1998).
4. Kurz, C. *et al.* Experimental protocol for high-fidelity heralded photon-to-atom quantum state transfer. *Nature Communications* **5**, 5527, https://doi.org/10.1038/ncomms6527 (2014).
5. Blinov, B. B., Moehring, D. L., Duan, L.-M. & Monroe, C. R. Observation of entanglement between a single trapped atom and a single photon. *Nature* **428**, 153–157, https://www.nature.com/nature/journal/v428/n6979/pdf/nature02377.pdf (2004).
6. Wilk, T., Webster, S. C., Kuhn, A. & Rempe, G. Single-Atom Single-Photon Quantum Interface. *Science* **317**, 488–490, http://www.ncbi.nlm.nih.gov/pubmed/17588899 (2007).
7. Gao, W. B., Fallahi, P., Togan, E., Miguel-Sanchez, J. & Imamoglu, A. Observation of entanglement between a quantum dot spin and a single photon. *Nature* **491**, 426–30, http://www.ncbi.nlm.nih.gov/pubmed/23151586 (2012).
8. De Greve, K. *et al.* Quantum-dot spinphoton entanglement via frequency downconversion to telecom wavelength. *Nature* **491**, 421, https://doi.org/10.1038/nature11577 (2012).
9. Schaibley, J. R. *et al.* Demonstration of quantum entanglement between a single electron spin confined to an InAs quantum dot and a photon. *Physical Review Letters* **110**, 1–5 (2013).
10. Vrijen, R. & Yablonovitch, E. A spin-coherent semiconductor photo-detector for quantum communication. *Physica E: Low-Dimensional Systems and Nanostructures* **10**, 569–575 (2001).
11. Kosaka, H. *et al.* Coherent Transfer of Light Polarization to Electron Spins in a Semiconductor. *Physical Review Letters* **100**, 096602, https://doi.org/10.1103/PhysRevLett.100.096602.0710.3847 (2008).
12. Kosaka, H. *et al.* Spin state tomography of optically injected electrons in a semiconductor. *Nature* **457**, 702–705, https://doi.org/10.1038/nature07729 (2009).
13. Fujita, T. *et al.* Single photoelectron spin detection and angular momentum transfer in a gate defined quantum dot **761**, 20, http://arxiv.org/abs/1504.03696 (2015).
14. Hanson, R., Kouwenhoven, L. P., Petta, J. R., Tarucha, S. & Vandersypen, L. M. K. Spins in few-electron quantum dots. *Rev. Mod. Phys.* **79**, 1217–1265, https://doi.org/10.1103/RevModPhys.79.1217 (2007).
15. Yoneda, J. *et al.* Fast electrical control of single electron spins in Quantum dots with vanishing influence from nuclear spins. *Physical Review Letters* **113**, 1–5 (2014).
16. Malinowski, F. K. *et al.* Notch filtering the nuclear environment of a spin qubit. *arXiv* 1601.06677, http://arxiv.org/abs/1601.06677 (2016).
17. Thalineau, R., Valentin, S. R., Wieck, A. D., Baeuerle, C. & Meunier, T. Interplay between exchange interaction and magnetic field gradient in a double quantum dot with two individual electron spin qubits. *Physical Review B* **90**, 075436 http://link.aps.org/doi/10.1103/PhysRevB.90.075436{\%}5Cn{\%}3CGotoISI{\%}3E://WOS:000344351700004 (2014).
18. Takakura, T. *et al.* Single to quadruple quantum dots with tunable tunnel couplings. *Applied Physics Letters* **104**, 1401.2212 (2014).
19. Delbecq, M. R. *et al.* Full control of quadruple quantum dot circuit charge states in the single electron regime. *Applied Physics Letters* **104**, 1–4 (2014).
20. Ito, T. *et al.* Detection and control of charge states in a quintuple quantum dot **193101**, 1–10, http://arxiv.org/abs/1604.04426 (2016).
21. Kosaka, H. *et al.* Single photoelectron trapping, storage, and detection in a field effect transistor. *Physical Review B* **67**, 045104, https://doi.org/10.1103/PhysRevB.67.045104 (2003).

22. Rao, D. S., Szkopek, T., Robinson, H. D., Yablonovitch, E. & Jiang, H. W. Single photoelectron trapping, storage, and detection in a one-electron quantum dot. *Journal of Applied Physics* **98**, 0410094 (2005).
23. Kuwahara, M., Kutsuwa, T., Ono, K. & Kosaka, H. Single charge detection of an electron created by a photon in a g-factor engineered quantum dot. *Applied Physics Letters* **96**, 10–13 (2010).
24. Pioda, A. *et al*. Single-shot detection of electrons generated by individual photons in a tunable lateral quantum dot. *Physical Review Letters* **106**, 146804, https://doi.org/10.1103/PhysRevLett.106.146804 (2011).
25. Fujita, T. *et al*. Nondestructive real-time measurement of charge and spin dynamics of photoelectrons in a double quantum dot. *Physical Review Letters* **110**, 266803, https://doi.org/10.1103/PhysRevLett.110.266803 (2013).
26. Morimoto, K. *et al*. Single photoelectron detection after selective excitation of electron heavy-hole and electron light-hole pairs in double quantum dots. *Physical Review B - Condensed Matter and Materials Physics* **90**, 085306, https://doi.org/10.1103/PhysRevB.90.085306 (2014).
27. Kwiat, P. G. *et al*. New high-intensity source of polarization-entangled photon pairs. *Physical Review Letters* **75**, 4337–4341 (1995).
28. Bitton, G., Grice, W. P., Moreau, J. & Zhang, L. Cascaded ultrabright source of polarization-entangled photons. *Physical Review A - Atomic, Molecular, and Optical Physics* **65**, 638051–638057, papers3://publication/uuid/A5F08072-6865-49E0-8042-15AF5B5A2ECBhttp://www.google.com/search?client=safari{\&}rls=10{_}7{_}4{\&}q=Ultrabright+Source+of+Polarization+Entangled+Photons{\&}ie=UTF-8{\&}oe=UTF-8papers3://publication/uuid/7E596713-914B-434D-91E7-AD31558CC924, 9810003 (2002).
29. Ciorga, M. *et al*. Addition spectrum of a lateral dot from coulomb and spin-blockade spectroscopy. *Phys. Rev. B* **61**, R16315–R16318, https://doi.org/10.1103/PhysRevB.61.R16315 (2000).
30. Elzerman, J. M. *et al*. Few-electron quantum dot circuit with integrated charge read out. *Phys. Rev. B* **67**, 161308, https://doi.org/10.1103/PhysRevB.67.161308 (2003).
31. Hanson, R. *et al*. Single-shot readout of electron spin states in a quantum dot using spin-dependent tunnel rates. *Phys. Rev. Lett.* **94**, 196802, https://doi.org/10.1103/PhysRevLett.94.196802 (2005).
32. Barthel, C. *et al*. Fast sensing of double-dot charge arrangement and spin state with a radio-frequency sensor quantum dot. *Phys. Rev. B* **81**, 161308, https://doi.org/10.1103/PhysRevB.81.161308 (2010).
33. Reilly, D. J., Marcus, C. M., Hanson, M. P. & Gossard, A. C. Fast single-charge sensing with a rf quantum point contact. *Applied Physics Letters* **91**, 1–4 (2007).
34. Kouwenhoven, L. P. *et al*. *Electron Transport in Quantum Dots*, 105–214, https://doi.org/10.1007/978-94-015-8839-3_4 (Springer Netherlands, Dordrecht, 1997).
35. Genet, C. & Ebbesen, T. W. Light in tiny holes. *Nature* **445**, 39–46, https://doi.org/10.1038/nature05350 (2007).
36. Barthel, C. *et al*. Fast sensing of double-dot charge arrangement and spin state with a radio-frequency sensor quantum dot. *Physical Review B - Condensed Matter and Materials Physics* **81**, 3–6 (2010).

Author Contributions
S.T. and A.O. conceived the study. S.R.V., A.L. and A.D.W. grew the quantum well wafer. K.K., M.L., S.M., T.F., and A.O. contributed to the device fabrication and constructed the measurement setup. K.K. and M.L. carried out the measurements. K.K., S.M. and S.T. analyzed the data and wrote the paper. S.T. and S.M. supervised the study.

Additional Information
Supplementary information accompanies this paper at https://doi.org/10.1038/s41598-017-16899-w.

Competing Interests: The authors declare that they have no competing interests.

Publisher's note: Springer Nature remains neutral with regard to jurisdictional claims in published maps and institutional affiliations.